Journal of Instrumentation

PAPER • **OPEN ACCESS**

Estimates of foil thickness, signal, noise, and nuclear heating of imaging bolometers for ITER

To cite this article: B.J. Peterson *et al* 2022 *JINST* **17** P06034

Published by IOP Publishing for Sissa Medialab

Received: *February 15, 2022*
Revised: *May 16, 2022*
Accepted: *May 16, 2022*
Published: *June 27, 2022*

Estimates of foil thickness, signal, noise, and nuclear heating of imaging bolometers for ITER

B.J. Peterson,[a,b,*] **T. Nishitani,**[c] **R. Reichle,**[d] **K. Munechika,**[e] **M.G. O'Mullane**[f] **and K. Mukai**[a,b]

[a] *National Institute for Fusion Science, 322-6 Oroshi-cho, Toki 509-5292, Japan*
[b] *SOKENDAI (Graduate University for Advanced Studies), 322-6 Oroshi-cho, Toki 509-5292, Japan*
[c] *Nagoya University, Furo-cho, Chikusa-ku, Nagoya 464-8603, Japan*
[d] *ITER Organization, Route de Vinon-sur-Verdon CS 90 046, St. Paul Lez Durance Cedex 13067, France*
[e] *Tokyo Institute of Technology, 2-12-1 Ookayama, Meguro-ku, Tokyo 152-8550, Japan*
[f] *Department of Physics, SUPA, University of Strathclyde, Glasgow G4 ONG, U.K.*

E-mail: peterson@nifs.ac.jp

Abstract: Imaging bolometers have been studied for ITER to serve as a complementary diagnostic to the resistive bolometers for the measurement of radiated power. Two tangentially viewing InfraRed imaging Video Bolometers (IRVB) could be proposed for an ITER equatorial port, one having a view of the entire plasma cross-section (core viewing) and one tilted down 43 degrees from the horizontal to view the divertor (divertor viewing). The IRVBs have 7 cm (horizontal) by 9 cm (vertical) Pt sensor foils, 6 mm × 6 mm apertures, 15 × 20 pixels and focal lengths of 7.8 cm and 21 cm, respectively. Using SANCO and SOLPS models for a 840 m^3 plasma radiating 67.3 MW, synthetic images from the IRVBs are calculated to estimate the maximum signal strengths to be 246 W/m^2 and 62 W/m^2, respectively. We propagate the X-ray energy spectra from the models through the synthetic diagnostics to give the photon energy spectrum for each IRVB pixel, which

*Corresponding author.

https://doi.org/10.1088/1748-0221/17/06/P06034

2022 JINST 17 P06034

are used to calculate the fraction of the power absorbed by the foil as a function of foil thickness. Using a criteria of >95% absorbed power fraction, we selected foil thicknesses of 30 μm and 10 μm, respectively. We used these thicknesses and assumed IR systems having 105 fps, 1024×1280 pixels and sensitivities of 15 mK, to calculate the IRVB sensitivities of 3.19 W/m^2 and 1.05 W/m^2, and signal to noise ratios of 77 and 59, respectively. Using the Monte Carlo Nuclear Particle code we calculated for the core viewing IRVB the foil heating by neutrons to be 1.0 W/m^2 and by gammas to be 117 W/m^2. This indicates that countermeasures may be needed to remove the nuclear heating signal.

KEYWORDS: Plasma diagnostics - interferometry, spectroscopy and imaging; Nuclear instruments and methods for hot plasma diagnostics

2022 JINST 17 P06034

Contents

2022 JINST 17 P06034

1 Introduction

Bolometry is an essential diagnostic for the measurement of the total plasma radiation, independent of wavelength, from a fusion reactor, which makes a significant contribution to the power balance [1]. Especially for the understanding of the plasma radiation distribution during impurity seeding [2], used to reduce the heat load on the divertor through enhanced radiation, two-dimensional (2D) radiation profiles, obtained through tomographic inversion of line averaged signals from collimated bolometer detectors [3]–[5], will play the main role. The resistive bolometer is a standard diagnostic and will be installed in ITER as the main bolometer diagnostic [6]. The resistive bolometers are typically installed in arrays distributed around a single poloidal cross-section to give the 2D radiation profile at that toroidal location [3].

As an alternative and complementary diagnostic, the InfraRed (IR) imaging Video Bolometer (IRVB) [7]–[9] is being considered for ITER. This diagnostic relies on an IR periscope and camera to image a thin metal foil, blackened with graphite, and mounted in a frame, which in turn images

the plasma through an aperture to give an image of the plasma radiation. In this way the broadband plasma radiation is absorbed by the foil and converted to IR radiation which is measured by the IR camera. The radiated power absorbed by the foil is calculated by using the 2D heat balance equation of the thin foil, including diffusive terms, the absorbed plasma radiation term and the blackbody radiation term [8], after proper calibration of the foil thermal and IR properties [8, 10]–[13]. In contrast to the resistive bolometers, the IRVBs use a tangential view and invoke the toroidal symmetry of the tokamak geometry to provide lines of sight viewing the entire plasma cross-section [14]. In previous work [15] the signal to noise ratio and foil thickness were considered for a single IRVB of arbitrary location viewing the entire plasma cross-section with a tangential view in ITER, assuming a foil viewing the plasma with no collimation for the estimate of the necessary foil thickness. In this work we have designed two IRVBs for ITER taking into consideration the fields of view, necessary foil thicknesses, sensitivities, and nuclear heating of the IRVB foil. In contrast to the previous work [15], we use realistic IRVB locations having the same aperture coordinates as existing IR thermal imaging diagnostic designs and determine the necessary foil thickness for each IRVB detector, including the effect of collimation. In this paper, in section 2 we introduce the two IRVBs, one having a tangential view of the entire cross-section and one having a view looking down into the divertor. In section 3 the synthetic radiation images for the IRVBs are derived from radiation models. Since the radiation models also include X-ray energy spectral information, we can use this to determine the energy spectrum of the radiation absorbed by each IRVB channel. Then this spectral information is used to determine the minimum foil thicknesses. Using these thicknesses, we can then calculate the sensitivity of the IRVBs and using the synthetic signals, calculate the signal to noise ratios. In section 4 a Monte Carlo Neutral Particle (MCNP) model is used to evaluate the heating of the foil by neutrons and gammas and compare with the expected signal and noise levels from section 3. In section 5 the paper will be summarized and concluded with a perspective on the applicability of the IRVB to ITER.

2 IRVB design

The IRVB designs consist of the locations of the apertures and foils and the dimensions of the foil and aperture camera and their resulting fields of view.

2.1 IRVB locations

The locations in ITER of the apertures of the two IRVBs, as given by the coordinates in table 1, are chosen to correspond to locations of the apertures of the planned Visible/Infrared Wide Angle Viewing System (Vis/IR EWAVS) views, with the idea that redundant Vis/IR EWAVS views could be replaced with IRVBs. The core viewing IRVB has a view which is horizontal and would replace the left-hand tangential view of the Vis/IR EWAVS system known as 12L and the divertor viewing IRVB is tilted down towards the divertor with the foil normal having and angle of 43° with the horizontal. It would replace the right-hand tangential view of the Vis/IR EWAVS system known as 12R. The fields of view are shown in figures 1 and 2, respectively.

2022 JINST 17 P06034

Table 1. Locations of foil and aperture centers for core and divertor viewing IRVBs in ITER coordinates.

	Aperture Center Position				Foil Center Position		
IRVB	X (m)	Y (m)	R (m)	Z (m)	X (m)	Y (m)	Z (m)
Core viewing	−5.8416	−6.2746	8.5729	0.47	−5.8443	−6.3525	0.47
Divertor Viewing	−5.8730	−6.2482	8.5751	0.82	−6.0445	−6.2941	0.9375

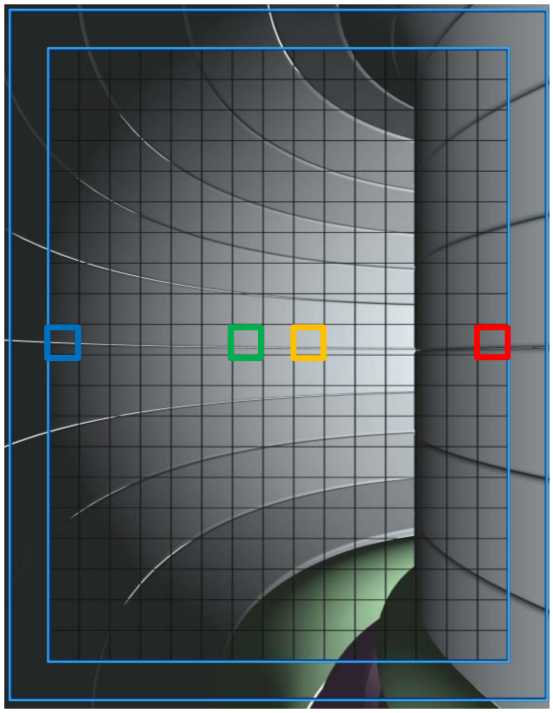

Figure 1. Field of view of core viewing IRVB. Black grid indicates bolometer channels and outer blue line is edge of frame. Colored squares are used to identifiy individual pixels.

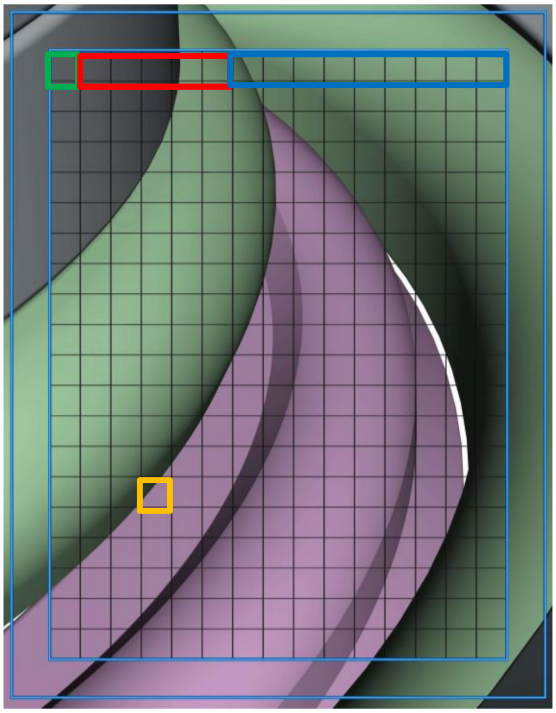

Figure 2. Field of view of divertor viewing IRVB. Black grid indicates bolometer channels and outer blue line is edge of frame. Colored squares are used to identifiy individual pixels or pixel groups.

2.2 IRVB design parameters

Each IRVB has a thin Pt foil mounted in a copper frame with exposed dimensions of 9 cm (vertical)× 7 cm (horizontal). This size is chosen due to the ready availability of foils having the dimensions 10 cm × 10 cm and in order to match the aspect ratio of the IR camera field of view. The thickness of the foil will be addressed in section 3.2. The field of view is limited to 8 cm × 6 cm to avoid using the edge IR pixels near the frame. Each foil is divided up numerically into 20 × 15 IRVB pixels (as shown in the field of view images in figures 1 and 2) having dimensions of 4 mm × 4 mm. The aperture sizes are 6 mm × 6 mm and the focal lengths (distances from foil to aperture), $l_{\text{ap-f}}$, are 78 mm for the core viewing IRVB and 210 mm for the divertor viewing IRVB. The aperture dimensions are chosen to be 1.5 times the linear dimensions of the bolometer pixels, which has been shown to be an effective trade-off between increased signal and reducing the overlap between channels which would degrade the accuracy of the 2D tomographic reconstruction [16]. Since the

2022 JINST 17 P06034

size of the pixel is related to the sensitivity, (as is discussed in section 3.3.1) and to the aperture size, which determines the signal strength (as is discussed in section 3.1.2), the pixel size (and thereby the number of pixels) is chosen in consideration to the signal to noise ratio which is determined in section 3.3.2. The planes of the apertures for the two IRVBs are parallel to the foils. For the core viewing IRVB, the aperture center is colinear with the normal to the foil center. For the divertor viewing IRVB, the aperture center is colinear to the normal emanating from a point on the foil 35 mm above the foil center in foil coordinates. This is done to increase the angle of incidence on the foil for those upper lines of sight which pass through the core part of the plasma, whence emanate the high energy x-rays. The increased angle of incidence of the sightline on the foil, θ, results in a longer path through the foil, which is more effective to stop the high energy x-rays from the core and thereby can permit a thinner foil (by a factor of $\cos\theta$) to be utilized, which will improve the sensitivity. This will be discussed and explained further in the next section regarding the determination of the foil thickness.

3 Determination of necessary foil thicknesses and estimation of signal to noise ratios

In a previous work, the necessary foil thickness was estimated by assuming the foil was exposed to the entire plasma without collimation [15]. This method however should result in an underestimation of the foil thickness. In this paper we consider the geometry of the pinhole camera and still consider the foil as a whole. This gives a better estimate of the necessary foil thickness than the previous work.

3.1 Calculation of synthetic images for IRVBs

The synthetic image data, P_{iE}, for each IRVB pixel, i, and x-ray energy level, E, are calculated from the plasma radiation model data, U_{jE}, for each plasma voxel, j, by using a geometry matrix, T_{ij}, (also known as a projection matrix) according to equation (3.1).

$$P_{iE} = \sum_j \frac{V_{ij}\Omega_{ij}}{4\pi} U_{jE} = \sum_j T_{ij} U_{jE} \,. \tag{3.1}$$

The calculation of the geometry matrices is carried out as described previously [15]. The radiation model data comes from the SANCO and SOLPS models [17] for the ITER standard 15 MA reference plasma scenario [18], which are introduced in the next subsection.

3.1.1 SOLPS and SANCO models

Two models of the plasma radiation are used in the calculation of the synthetic images. The first of these is the SANCO model which provides a 1D (minor radial) model of the plasma radiation consisting of 30 annular regions inside the last closed flux surface. The second is the 2D SOLPS model which divides up the edge and divertor region into 8866 conformal grid elements. These are both resampled to a 2D (major radius, R, height, Z) grid having 219 (horizontal, 4.02 m $<$ R $<$ 8.4 m) $\times$ 465 (vertical, -4.58 m $<$ Z $<$ 4.72 m) 2 cm square pixels. The impurity mix used in the models is 2% Be and 10^{-5} W.

2022 JINST 17 P06034

3.1.2 Estimation of signal levels for IRVBs

Two methods are used to estimate the signal levels of the IRVBs. The first of these is a rough estimate of the incident radiated power, P_{signal}, and power density, S_{signal}, based on equation (3.2) [15],

$$S_{\text{signal}} = \frac{P_{\text{signal}}}{A_{\text{bol}}} = \frac{A_{\text{bol}} A_{\text{ap}} \cos^4 \theta P_{\text{rad}} l_{\text{plasma}}}{A_{\text{bol}} 4\pi l_{\text{ap-f}}^2 V_{\text{plasma}}} \tag{3.2}$$

where A_{bol} is the area of the bolometer pixel, A_{ap} is the area of the aperture, P_{rad} is the total plasma radiated power, l_{plasma} is the length of the sightline through the plasma and V_{plasma} is the plasma volume. The quantities used in the estimation of equation (3.2) and the resulting estimated signal levels are shown in table 2.

Table 2. IRVB and plasma parameters used in rough estimate of IRVB signal level.

IRVB	A_{bol} (mm^2)	A_{ap} (mm^2)	$l_{\text{ap-f}}$ (cm)	θ (°)	l_{plasma} (m)	P_{rad} (MW)	V_{plasma} (m^3)	S_{signal} (W/m^2)
Core viewing	16	36	7.8	20	10	67.27	1049.3	235
Divertor Viewing	16	36	21	10	5	67.27	1049.3	19.6

A more accurate estimation of the signal level is given from the radiation models by using equation (3.1) and summing over all the energy channels to give the synthetic images shown in figures 3 and 4 for the core and divertor viewing IRVBs, respectively. The maximum signal levels are then given as 246 and 62 W/m^2, respectively, which is comparable with the rough estimate in the case of the core viewing IRVB, but is approximately 3 times higher than the rough estimate in the case of the divertor viewing IRVB. This discrepancy is due to the use of the total radiated power for the radiation from the divertor which should be much higher. In any case the synthetic data from the SOLPS model should give the most accurate estimate since it takes into account the very localized radiated power density data from the SOLPS model and the field of view geometry of the diagnostic.

3.2 Determination of necessary foil thicknesses for IRVBs

If the foil is too thin, then high energy photons from the core will not be absorbed by the foil and the bremsstrahlung power radiated by the core will not be adequately measured. On the other hand, the thicker the foil, the less sensitive the diagnostic is, as will be explained in section 3.3.1, when the relevant equation for the IRVB sensitivity is introduced. Therefore, we should choose the foil to be as thin as possible for the sake of high sensitivity, but still thick enough to be able to absorb a high enough fraction of the high energy photons to make an accurate estimate of the total and locally radiated power. In addition, the strength of the free-standing foil should provide another constraint on the minimum thickness of the foil. Both the strength and photon stopping power of the foil are dependent on the foil material, but we have studied that previously and determined that Pt is the most suitable foil material [19]. Therefore, Pt will be the only foil material considered in this study. In order to consider the necessary thickness to stop the high energy photons we can use the x-ray energy spectrum included in the radiation models to calculate the energy spectrum of the incident photons on each bolometer pixel. And then we can calculate the fraction of the power absorbed by each pixel as a function of foil thickness. Finally, by applying a criterion for the absorbed power fraction we can determine the necessary foil thickness.

2022 JINST 17 P06034

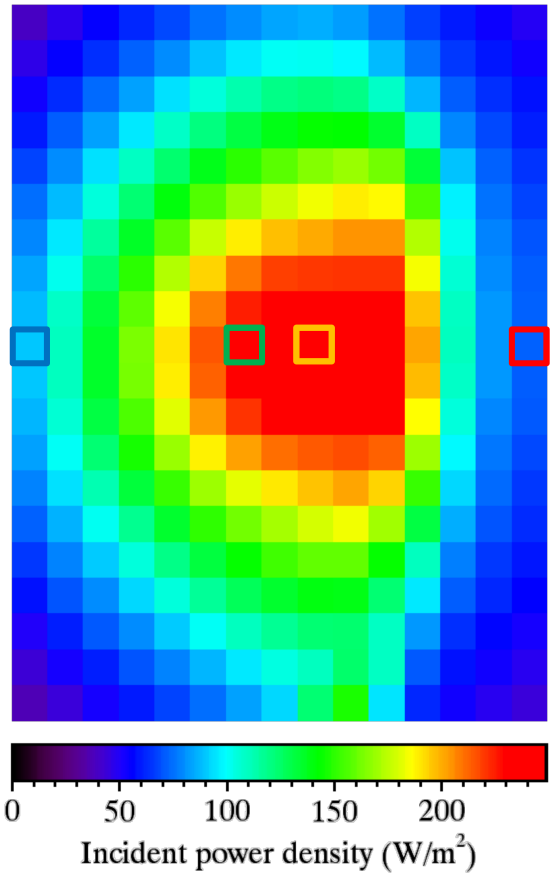

Figure 3. Syntheitc image from SOLPS and SANCO models of incident radiated power density for core viewing IRVB. Colored squares are used to identifiy individual pixels.

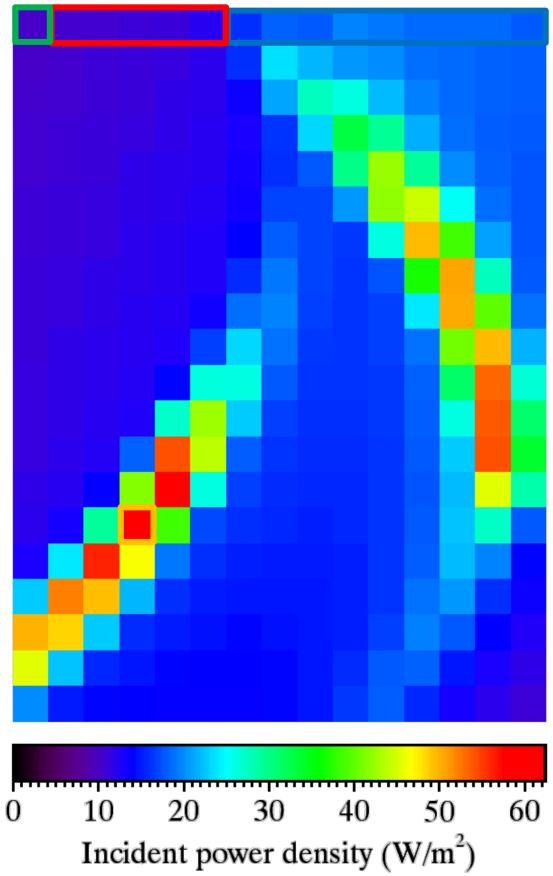

Figure 4. Syntheitc image from SOLPS and SANCO models of incident radiated power density for divertor viewing IRVB. Colored rectangles are used to identifiy individual pixels or pixel groups.

3.2.1 Calculation of energy spectra of photons incident on each IRVB pixel

By using equation (3.1), including the energy spectra data of the SOLPS and SANCO models, we can calculate the energy spectra of the incident photons on each IRVB pixel. The models have energy spectra divided into 236 channels ranging from 1 eV to 100 keV. The energy spectrum data is resampled into 94 channels with the power from all of the channels below 1 keV being combined into the 1 keV channel. Energy spectra for 4 channels from the core viewing IRVB are shown in figure 5. The four channels are color-coded and their positions are shown in figures 1 and 3. Blue is the outboard channel, green is the channel with the highest energy, yellow is the channels with the highest power and red is the inboard channel.

3.2.2 Calculation of fraction of power absorbed by each IRVB pixel versus foil thickness and estimation of necessary foil thicknesses

Using the mass attenuation coefficient m/r data from NIST [20] (where μ is the attenuation coefficient and ρ is the mass density) and ρ for Pt we use equation (3.3) to calculate the variation in the fraction of the incident radiated power, P_0, absorbed by the foil, P, for each IRVB channel in terms

2022 JINST 17 P06034

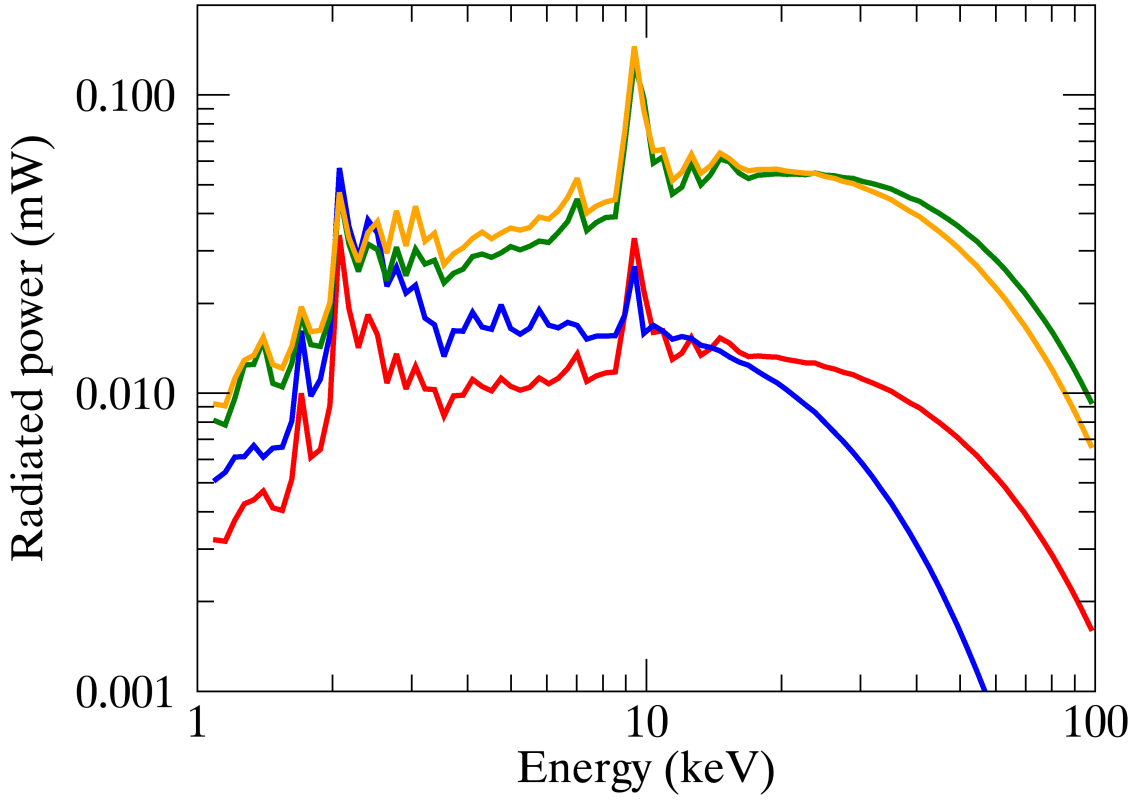

Figure 5. Incident radiated power versus photon energy for 4 channels from the core viewing IRVB as predicted by SOLPS and SANCO radiation models. The location of the four channels is shown by the colored squares in figures 1 and 3.

of the foil thickness, t_f, taking into account the angle of incidence, θ, of the line of sight on the foil.

$$\frac{P}{P_0}(t_f) = \frac{1}{P_0}\sum_E P(E)\left\{1 - e^{-\frac{\mu}{\rho}(E)\rho t_f/\cos\theta}\right\}. \tag{3.3}$$

The NIST data ranges from 1 to 100 keV in 40 energy levels. This was resampled to match the SANCO/SOLPS energy levels. The results are plotted for the four channels indicated in figures 1 and 3 and for the total foil for the core viewing IRVB as shown in figure 6.

For the divertor viewing IRVB a similar plot is shown in figure 7. Energy levels and, consequently, necessary foil thicknesses are much lower than those of the core viewing IRVB due to the field of view tilted down towards the divertor and therefore missing much of the high energy photons form the core. The color coding is similar to that of figure 6 with the corresponding pixels being indicated by color outlined regions in figures 2 and 4. The pixels with the most energetic photons are from the upper row of pixels having the longest sightlines through the core region, with the pixel viewing the most energetic photons being on the inboard side and once again being indicated by the green square. The other inboard pixels are indicated by the red rectangle and the outboard pixels are indicated by the blue rectangle. The pixel with the highest power is viewing the divertor and is once again indicated by a yellow square. The cyan line is again for the total foil taken as one pixel.

2022 JINST 17 P06034

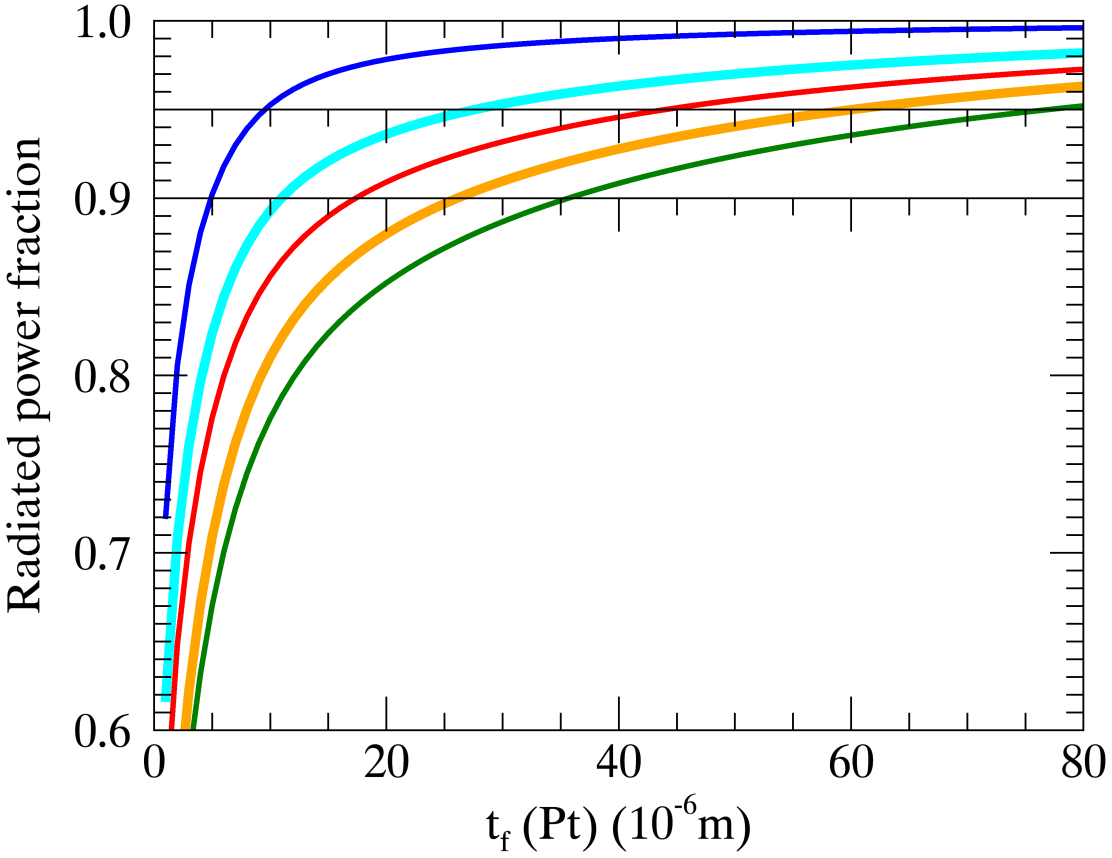

Figure 6. Fraction of incident radiated power absorbed by foil versus foil thickness for 4 channels from the core viewing IRVB as predicted by SOLPS and SANCO radiation models. The location of the four channels is shown by the colored squares in figures 1 and 3, which correspond to the line colors. The cyan line indicates the value for the total foil.

Using the criteria of absorption of 95% of the incident power for the foil as a whole (cyan line) we select a 30 µm Pt foil for the core viewing IRVB and a 10 µm foil for the divertor viewing IRVB.

3.3 Estimation of sensitivities and signal to noise ratios for IRVBs

Now that we have determined the necessary foil thicknesses, we can look at the sensitivities of the IRVBs in terms of the noise equivalent power densities and compare those to the power densities estimated from the synthetic signals based on the radiation models and the rough estimate form equation (3.2) to estimate the signal to noise ratio as a figure of merit of the diagnostic effectiveness of the IRVBs.

3.3.1 Calculation of noise equivalent power densities for IRVBs

The noise equivalent power density (NEPD), S_{IRVB}, is a measure of the sensitivity of the IRVB that was previously derived by propagating the error in the IR camera measurement of the foil temperature through the power balance equation of the foil [8]. As the NEPD decreases the

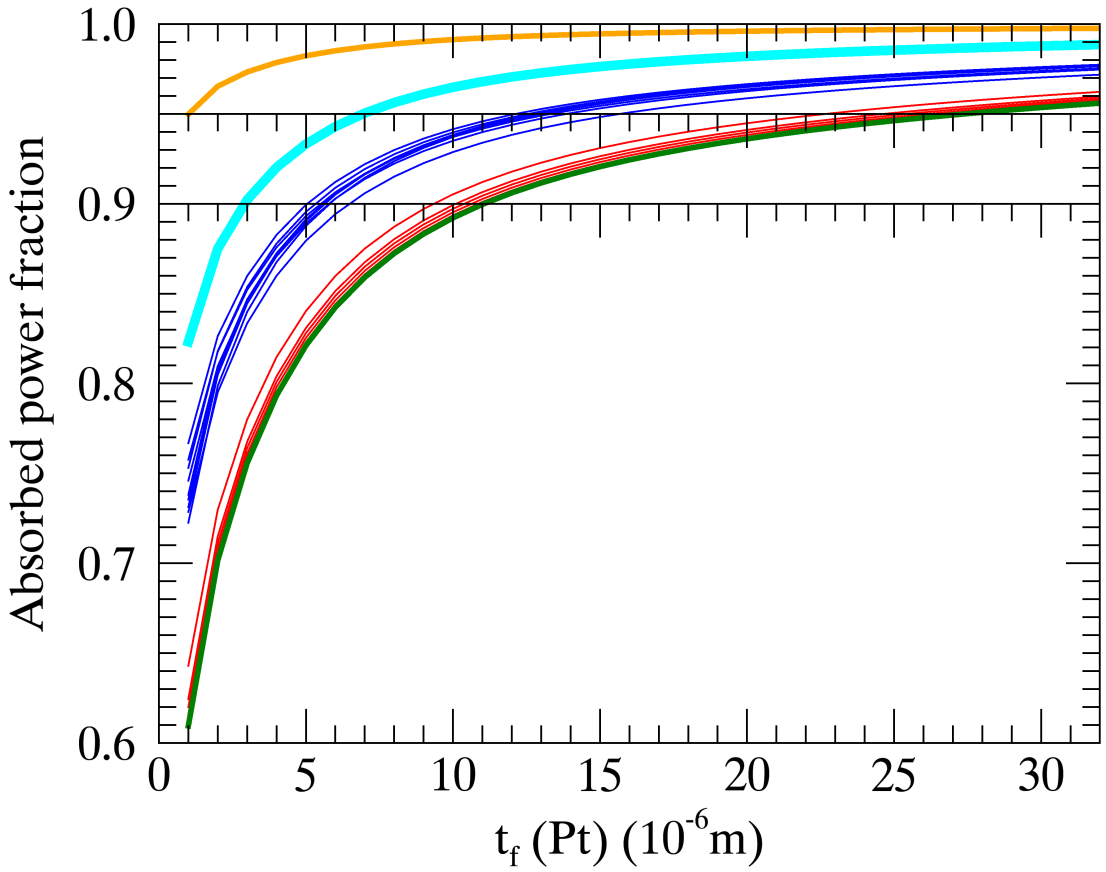

Figure 7. Fraction of incident radiated power absorbed by foil versus foil thickness for channels from the divertor viewing IRVB as predicted by SOLPS and SANCO radiation models. The location of the channels is shown by the colored rectangles in figures 2 and 4, which correspond to the line colors. The cyan line indicates the value for the total foil.

sensitivity increases. The NEPD is given by equation (3.4)

$$S_{\mathrm{IRVB}} = \frac{\eta_{\mathrm{IRVB}} N_{\mathrm{bol}}}{A_{\mathrm{f}}} = \frac{\sqrt{10} k t_{\mathrm{f}} \sigma_{\mathrm{IR}}}{\sqrt{f_{\mathrm{IR}} N_{\mathrm{IR}}}} \sqrt{\frac{N_{\mathrm{bol}}^3 f_{\mathrm{bol}}}{A_{\mathrm{f}}^2} + \frac{N_{\mathrm{bol}} f_{\mathrm{bol}}^3}{5\kappa^2}} \tag{3.4}$$

with η_{IRVB} the noise equivalent power, N_{bol} the number of bolometer pixels, A_{f} the foil area, k the foil thermal conductivity, σ_{IR} the noise equivalent temperature difference (NETD) of the IR camera measurement, f_{IR} the frame rate of the IR camera measurement, N_{IR} the number of IR camera pixels, f_{bol} the frequency of the bolometer measurement and κ the foil thermal diffusivity. Here the dependence of the sensitivity on the foil thickness clearly can be seen. In addition, it can be seen that many trade-offs may be made between temporal ($1/f_{\mathrm{bol}}$) and spatial resolution ($\sim 1/N_{\mathrm{bol}}$) also depending on the parameters of the IR system (f_{IR}, N_{IR}, σ_{IR}). The hard upper limit for f_{bol} is f_{IR}, but a lower value may be taken through frame averaging for improved sensitivity at the expense of temporal resolution. In the same way, the foil area, is divided up numerically into the number of bolometer pixels by averaging over the number of IR camera pixels. Reducing N_{bol} results in improved sensitivity at the cost of bolometer channels and spatial resolution. The selected design parameters and the resulting NEPDs are shown in table 3.

2022 JINST 17 P06034

The NETD of the IR camera system, σ_{IR}, is conservatively estimated to be 15 mK. This is based on our experience with the IRVB on JT-60U which had an NETD of 11.2 mK and an IR transmission of 0.908 [9].

3.3.2 Estimation of signal to noise ratios for IRVBs

When compared with the rough estimate of the signal level provided by equation (3.2) the signal to noise ratios (SNR) for the core viewing and divertor viewing IRVBs are 74 and 19, repectively. Compared with the synthetic image data from the radiation models, the SNRs are 77 and 59, respectively. The relatively low level of the rough estimate of the signal from eq. (3.2) for the divertor viewing IRVB may be due to the assumption of a uniformly radiating plasma while the radiation from the divertor region is highly localized as was previously described.

4 Nuclear heating of IRVB foil

One cause of concern regarding operation of an IRVB on ITER or any fusion reactor would be the nuclear heating of the foil by neutrons and gammas, both the prompt gammas coming directly from the plasma and secondary gammas produced by interactions between the neutrons and the surrounding machine structure. Therefore, in this section we investigate the extent of this heating by modeling with the Monte Carlo Nuclear Particle (MCNP) code.

4.1 MCNP model

The simplified ITER MCNP model includes the vacuum vessel, shielding blankets and structure of one 20° toroidal section as shown in the 3-dimensional schematic view in figure 8. The core viewing IRVB is modelled as a 213 mm long, stainless steel (SS) cylinder having an inner diameter of 135 mm and an outer diameter of 155 mm as shown in figure 9. The foil is mounted in the cylinder between two circular copper frames, each frame having a thickness of 10 mm. The exposed part of the foil has a diameter of 90 mm. The circular aperture plate attached to the end of the cylinder is SS with a thickness of 10 mm and a circular aperture of 6.8 mm in diameter giving it the same area as that of the square aperture of the core viewing IRVB. The positions of the foil and aperture are the same as those given for the core viewing IRVB in table 1. The thickness of the foil is modelled as a 3 mm thick Pt foil with 1/100 of the density to give it the same mass as the 30 µm thick Pt foil of the design. The foil is divided into 5 annular sections with boundaries at radii of 5, 15, 25, 35 and 45 mm. In this calculation MCNP version 6 [21] and the FENDL-3.1 nuclear data file [22] are used.

4.2 Estimation of IRVB foil heating by neutrons and gammas

The results of the MCNP modelling are given in tables 3 and 4 for comparison with the IRVB estimated signal and noise levels. The neutron heating of the foil is negligible when compared with the NEPD. The heating of the foil by gammas, however, is more than 100 times that of the neutrons and is ~50% of the maximum signal from the synthetic image. This heating is thought to be due to secondary gammas as a similar result is obtained when the there is no aperture. The radial variation of the heating on the foil is negligible compared to the error in the modeling results.

2022 JINST 17 P06034

Table 3. IR system parameters, IRVB parameters, IRVB signal and noise levels, signal to noise ratios, nuclear heating levels.

Parameter IRVB	units	Core viewing	Divertor viewing
IR System Parameters			
Number of pixels		1024×1280	
f_{IR}	1/s	105	
σ_{IR}	°mK	15	
IRVB Parameters			
N_{IR}		1,310,720	
N_{bol}	H × V	15×20	
f_{bol}	1/s	100	
A_f	cm^2	6×8	
t_f	µm	30	10
Signal and Noise Levels, Signal to Noise Ratios			
S_{IRVB} (eq. (3.4))	W/m^2	3.19	1.05
S_{signal} (eq. (3.2))	W/m^2	235	19.6
SNR		73.8	18.6
S_{core} (SANCO)	W/m^2	245	18.3
S_{edge} (SOLPS)	W/m^2	67	49.7
$S_{total} = S_{core} + S_{edge}$	W/m^2	246	61.8
SNR		77	59
Nuclear Heating Levels			
$S_{neutron}$	W/m^2	0.9–1.0 ± 6%	—
S_{gamma}	W/m^2	111–117 ± 8%	—
S_{gamma}/S_{total}		~0.47	—

5 Conclusions

In this paper we have shown that IRVBs for core and divertor views can be designed with adequate sensitivity. However, this estimate is based on conservative assumptions about the sensitivity of the IR system, represented by σ_{IR}. In the future this sensitivity should be determined through design of the IR system and we should address how this sensitivity is affected by nuclear heating of the IR optics. Also, while we expect to actively cool the IRVBs in ITER, the effect of an operating temperature above room temperture should be investigated as temperatures up to 350°C are expected. The sensitivity of the IRVB has been shown to increase with temeprature [23], therefore the estimates that we have given for room temperature should be conservative and greater singal to noise ratios should be expected for higher operating temperatures. Evaluation of the

2022 JINST 17 P06034

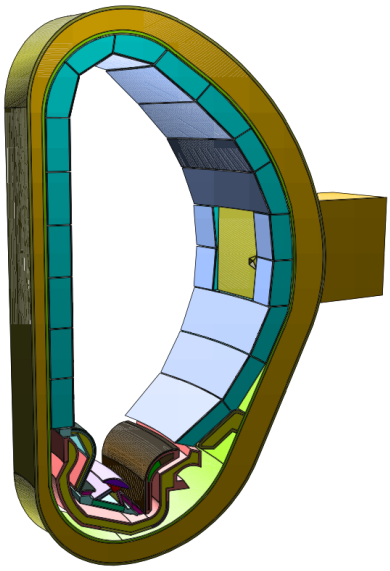

Figure 8. Three-dimensional image of 20° toroidal section MCNP model of ITER with IRVB.

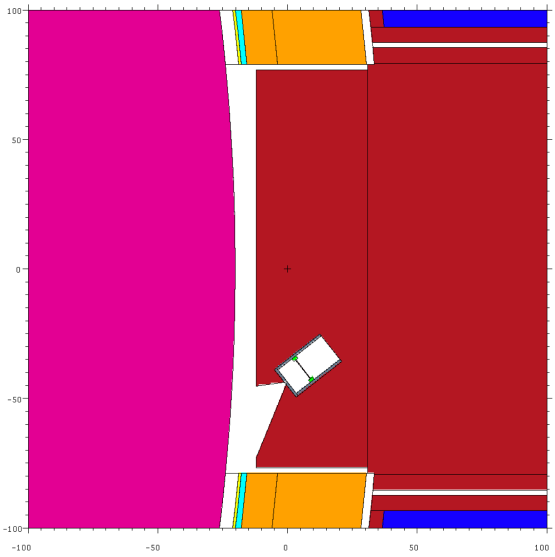

Figure 9. Horizontal cut image of top view of IRVB in ITER port plug MCNP model with plasma region shown in pink.

Table 4. Radial variation in heating of a 30 micron Pt foil by neutrons and gammas in ITER.

region	heating rate (W/m^2)					
r (mm)	neutron	error	gamma	error	total	error
35–45	0.915	±0.002	116	±2	117	±2
25–35	0.944	±0.003	116	±7	116	±7
15–25	0.976	±0.004	112	±3	113	±3
5–15	0.990	±0.006	111	±4	112	±4
0–5	1.01	±0.02	117	±9	118	±9

various effects of heating on the IR system could be evaluated by combined ZEMAX, ANSYS and MCNP modelling as part of the optical design of the diagnostic.

Also a better estimate than that given by a previous study [15] of the necessary foil thickness was made by utilising the actual fields of view of the IRVBs and the energy spectra of the radiation models. Our criteria of 95% capture of the incident power by the foil is still somewhat arbitrary and actually gave necessary foil thickenss of ~7 µm and ~27 µm for the divertor and core viewing IRVBs, respectively. However, we chose thicknesses of 10 µm and 30 µm, respectively, since we have not yet identified a foil producer that will provide a custom thickness and the commercially available thicknesses in a 10 cm × 10 cm Pt foil are 2.5, 10, 20, 25, 30 and 50 µm. Also, when considering the minimum safe thickness, with regard to the strength of the foil, experience indicates that we may not want to use a foil thinner than 10 µm, but this limit should also be determined more empirically through foil testing. A more detailed estimate of the foil thickness could be obtained through tomographic modelling to determine what percentage of the total radiated power is not

2022 JINST 17 P06034

measured as the the foil thickness is changed. In addition, tomographic modelling would give us a measure of the spatial resolution and how this could be improved for the divertor region with the addition of the divertor viewing IRVB. Therefore, we plan to carry out such modelling in the future.

With regard to the nuclear heating of the foil, this work has shown significant heating by secondary gammas. Several possibilites exist for the removal of this signal from the measurement depending on the nature of this heating. If the heating is uniform on the foil or has a reproducible and scalable dependence on the location in the foil, then we could place a plate over one of the edge pixels of the foil, blocking it from the incoming radiation. The signal from this pixel would then be used to measure the gamma heating in order to subtract it off, leaving the radiation signal. It might be best to have such a blind channel in each corner of the foil to monitor the spatial variation of the nuclear heating across the foil. If this heating distribution is not the case, then another possiblity would be to use a shutter on the aperture to periodically remove the radiation portion of the signal, leaving the gamma heating portion of the signal to be subtracted off. This, however, would require a shutter that would be operated much more frequently than the current standard for ITER shutters and would require more shutter R&D to insure reliability over the lifetime of the machine. In order to investigate these possibilities, more detailed MCNP modelling of the the foil will be necessary.

In addition to the plasma radiation and nuclear heating, charge exchange neutrals and stray microwave radiation should heat the foil and contribute to the signal. The stray microwave radiation is difficult to estimate, but could be reduced by using a mesh on the aperture (which would reduce the signal) and/or absorbing baffles inside the bolomter camera in the space between the aperture plate and the foil. The fraction of energy lost by charge exchange is estimated to be less than 15% in ITER [24].

In conclusion, based on the current work, we feel that the IRVB could be a viable diagnostic to complement the resistive bolometers currently planned for ITER, but much design and prototype testing remains to be done.

Acknowledgments

This work was completed with support from NIFS budget NIFS16ULHH026 and with support for Profs. Peterson and Nishitani from the ITER Scientist Fellowship Program.

Disclaimer: “the views and opinions expressed herein do not necessarily reflect those of the ITER Organization”.

Data availability: the data that support the findings of this study are available from the corresponding author upon reasonable request.

References

[1] A.J. Donne et al., *Chapter 7: Diagnostics*, *Nucl. Fusion* **47** (2007) S337.

[2] A. Kallenbach et al., *Impurity seeding for tokamak power exhaust: from present devices via ITER to DEMO*, *Plasma Phys. Contr. Fusion* **55** (2013) 124041.

[3] A.W. Leonard, W.H. Meyer, B. Geer, D.M. Behne and D.N. Hill, *2D tomography with bolometry in DIII-D*, *Rev. Sci. Instrum.* **66** (1995) 1201.

2022 JINST 17 P06034

[4] L.C. Ingesson, B. Alper, B.J. Peterson and J.-C. Vallet, *Chapter 7: Tomography diagnostics: Bolometry and soft-x-ray detection*, *Fusion Sci. Technol.* **53** (2008) 528.

[5] J. Jang et al., *Tomographic reconstruction of two-dimensional radiated power distribution during impurity injection in KSTAR plasmas using an infrared imaging video bolometer*, *Curr. Appl Phys.* **18** (2018) 461.

[6] H. Meister et al., *Bolometer developments in diagnostics for magnetic confinement fusion*, 2019 *JINST* **14** C10004.

[7] B.J. Peterson, *Infrared imaging video bolometer*, *Rev. Sci. Instrum.* **71** (2000) 3696.

[8] B.J. Peterson, A.Y. Kostrioukov, N. Ashikawa, M. Osakabe and S. Sudo, *Calibration and sensitivity of the infrared imaging video bolometer*, *Rev. Sci. Instrum.* **74** (2003) 2040.

[9] B.J. Peterson et al., *Development of imaging bolometers for magnetic fusion reactors (invited)*, *Rev. Sci. Instrum.* **79** (2008) 10E301.

[10] R. Sano, B.J. Peterson, E.A. Drapiko, D.C. Seo, Y. Yamauchi and T. Hino, *Foil calibration for IR imaging bolometer by laser irradiation*, *Plasma Fusion Res.* **7** (2012) 2405039.

[11] S.N. Pandya et al., *Calibration of a thin metal foil for infrared imaging video bolometer to estimate the spatial variation of thermal diffusivity using a photo-thermal technique*, *Rev. Sci. Instrum.* **85** (2014) 054902.

[12] K. Mukai, B.J. Peterson, S.N. Pandya and R. Sano, *In situ calibration of an infrared imaging video bolometer in the large helical device*, *Rev. Sci. Instrum.* **85** (2014) 11E435.

[13] K. Mukai, B.J. Peterson, S. Takayama and R. Sano, *In situ calibration of the foil detector for an infrared imaging video bolometer using a carbon evaporation technique*, *Rev. Sci. Instrum.* **87** (2016) 11E124.

[14] B.J. Peterson et al., *Signal to noise ratio of upgraded imaging bolometer for KSTAR*, *Rev. Sci. Instrum.* **89** (2018) 10E115.

[15] B.J. Peterson, R. Reichle, S. Pandya, M.G. O'Mullane and K. Mukai, *Consideration of signal to noise ratio for an imaging bolometer for ITER*, *Rev. Sci. Instrum.* **92** (2021) 043534.

[16] R. Sano, K. Mukai, B.J. Peterson, M. Fukumoto and K. Hoshino, *Conceptual design of imaging bolometer for use of computed tomography in JT-60SA*, *Rev. Sci. Instrum.* **88** (2017) 053506.

[17] M.G. O'Mullane, *Energy resolved radiated power simulations for ITER bolometer study — compatible core and edge predictions*, private communication (2016).

[18] A.R. Polevoi et al., *ITER confinement and stability modelling*, *J. Fusion Res. Series* **5** (2002) 82.

[19] R. Sano, B.J. Peterson, E.A. Drapiko, Y. Watanabe, Y. Yamauchi and T. Hino, *Thermal characteristics of foils for an imaging bolometer*, *Plasma Fusion Res.* **6** (2011) 2406076.

[20] J.H. Hubbell and S.M. Seltzer, *Tables of X-Ray Mass Attenuation Coefficients and Mass Energy-Absorption Coefficients (version 1.4)*, National Institute of Standards and Technology, Gaithersburg, MD, U.S.A. (2004) [https://doi.org/10.18434/T4D01F].

[21] D.B. Pelowits ed., *MCNP6 user's manual — Version 1.0*, Los Alamos National Laboratory, Los Alamos, NM, U.S.A. (2013) [LA-CP-13-00634].

[22] Nuclear Data services, International Atomic Energy Agency, (2022) https://www-nds.iaea.org/fendl/.

[23] E.A. Drapiko, B.J. Peterson, J. Kodaira and N. Ashikawa, *Advantages of high temperature operation of an imaging bolometer*, *J. Plasma Fusion Res. Series* **8** (2009) 659.

[24] D. Post, J. Abdallah, R.E.H. Clark and N. Putvinskaya, *Calculations of energy losses due to atomic processes in tokamaks with applications to the international thermonuclear experimental reactor divertor*, *Phys. Plasmas* **2** (1995) 2328.

2022 JINST 17 P06034